

RESEARCH ARTICLE | MARCH 19 2024

Epitaxial growth of Nd_2O_3 layers on virtual SiGe substrates on Si(111)

H. Genath ; M. A. Schubert ; H. L. Yamtomo ; J. Krügener ; H. J. Osten 

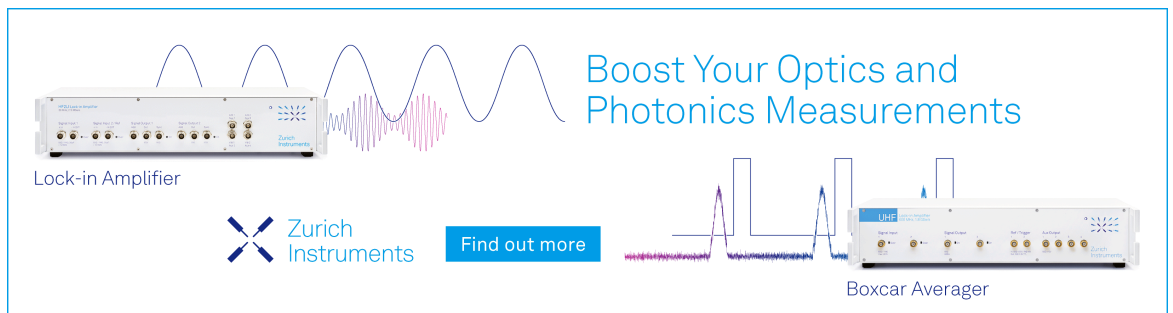


J. Appl. Phys. 135, 115302 (2024)

<https://doi.org/10.1063/5.0191350>



CrossMark



Boost Your Optics and Photonics Measurements

Lock-in Amplifier

Zurich Instruments

Find out more

Boxcar Averager

Epitaxial growth of Nd_2O_3 layers on virtual SiGe substrates on Si(111)

Cite as: J. Appl. Phys. **135**, 115302 (2024); doi: [10.1063/5.0191350](https://doi.org/10.1063/5.0191350)

Submitted: 13 December 2023 · Accepted: 4 March 2024 ·

Published Online: 19 March 2024



H. Genath,^{1,a)} M. A. Schubert,² H. L. Yamtomo,¹ J. Krügener,^{1,3} and H. J. Osten^{1,3}

AFFILIATIONS

¹Institute of Electronic Materials and Devices, Leibniz Universität Hannover, Schneiderberg 32, 30167 Hannover, Germany

²IHP-Leibniz-Institut für Innovative Mikroelektronik, Im Technologiepark 25, 15236 Frankfurt, Germany

³Laboratory of Nano and Quantum Engineering, Leibniz Universität Hannover, Schneiderberg 39, 30167 Hannover, Germany

^{a)}Author to whom correspondence should be addressed: genath@mbe.uni-hannover.de

ABSTRACT

This study explores the growth and structural characteristics of Nd_2O_3 layers on virtual germanium-rich SiGe substrates on Si(111). We focus on the emergence of the hexagonal phase depending on the stoichiometry of the virtual substrate. X-ray diffraction measurements reveal a hexagonal phase when Nd_2O_3 is grown directly on Si(111), while growth on Ge leads to a cubic oxide structure. On SiGe layers, the growth of the oxide results in a mixed phase containing hexagonal and cubic regions, regardless of the Ge content. The cubic structure grown on virtual Ge substrates exhibits strong tensile strain, while layers grown on SiGe layers show no strain. *In situ* growth control via electron diffraction shows a dependence of the oxide structure of the surface reconstruction of the virtual substrate. Growth on a 7×7 reconstruction leads to hexagonal parts on Si-based substrates, while growth on $c(2 \times 8)$ results in cubic oxide growth on Ge. Furthermore, oxide layers grown on virtual SiGe substrates form an interfacial silicate layer. The thickness of the interfacial layer is influenced by the Si content and the structure of the oxide layer enabling oxygen diffusion pathways.

© 2024 Author(s). All article content, except where otherwise noted, is licensed under a Creative Commons Attribution (CC BY) license (<https://creativecommons.org/licenses/by/4.0/>). <https://doi.org/10.1063/5.0191350>

I. INTRODUCTION

The integration of materials like germanium and silicon germanium on silicon is attractive for several reasons. These materials not only enable high-mobility channels with very high Ge content while mitigating parasitic effects like drain-induced barrier lowering^{1–4} but also the incorporation of optical devices in Si complementary metal-oxide-semiconductor (CMOS) devices.^{5–7} Ge and germanium-rich $\text{Si}_{1-x}\text{Ge}_x$ layers are known to have high intrinsic electron mobilities and especially high hole mobilities, making them suitable for CMOS devices.^{8–11} However, while p-type Ge-based devices have performed reasonably well, especially n-type Ge-based devices fall short of expectations.^{9,12}

The successful integration of Ge-based devices still faces substantial challenges. These challenges involve issues at the Ge/metal interface, which suffers from Fermi level pinning, and more critically, the poor interface quality between oxides and SiGe or Ge layers.^{9,11,13} Despite the initially lower number of dangling bonds at the interface in the Ge/ GeO_2 system compared to the Si/ SiO_2 system, the inability to passivate Ge dangling bonds with hydrogen

has rendered interface control at Ge interfaces quite difficult.^{12,14–16}

These unpassivated Ge dangling bonds contribute to the high density of interface states, degrading device performances.^{7,12} Even in SiGe-based devices, the high density of interface states is associated with undesired GeO_x formation at the high-k oxide (e.g., HfO_2) and SiGe interface.^{11,14}

The selection of an appropriate surface orientation can increase the charge carrier mobility further¹⁷ and enhance the n-type MOS performance for Ge-based transistors.^{18–21} The (111) orientation exhibits the highest electron mobility²² among the commonly used surface orientations and also demonstrated superior capacitance–voltage characteristics and a lower density of interface states in Ge-based MOS structures.^{17,18} Achieving a high-quality interface strongly depends on Ge surface passivation. Promising candidates for sufficient passivation are the rare-earth oxides (REOs) like Gd_2O_3 and CeO_2 that have shown a low density of interface states on Ge.^{9,10,23,24}

Among the REOs, Nd_2O_3 is known to exhibit two polymorphs which are the cubic bixbyite C-type with space group $Ia\bar{3}$ (Mn_2O_3

22 March 2024 06:55:37

type of structure) and the hexagonal A-type with space group $P\bar{3}m1$ (La_2O_3 type of structure).^{25,26} The cubic phase of Nd_2O_3 closely matches the lattice of $\text{Si}_{0.48}\text{Ge}_{0.52}(111)$. The growth of this cubic phase in an A/B stacking on Si(111) has shown a promising dielectric constant exceeding 14, with expectations of an even higher dielectric constant of around 27 when the transition to the hexagonal phase can be achieved.^{27,28}

For other rare-earth oxides, it has been demonstrated that their phase can be altered by the influence of pressure, growth conditions, and stress.^{29–34} To investigate the effects of stress, the growth of Nd_2O_3 layers on germanium-rich $\text{Si}_{1-x}\text{Ge}_x$ layers enables a systematic variation of the surface lattice parameter.

The focus of this study is on the structural characterization and growth of Nd_2O_3 layers on germanium-rich $\text{Si}_{1-x}\text{Ge}_x$ layers with $0.55 < x \leq 1$ on Si(111) substrates. We research the influence of tensile strain on Nd_2O_3 growth by varying the Ge content of the virtual $\text{Si}_{1-x}\text{Ge}_x$ substrate and investigate potential phase transitions. In addition to varying the surface lattice parameter, the thickness of the oxide layer is altered. All samples are particularly analyzed regarding strain and phase in the oxide layer and interfacial layer formation.

II. EXPERIMENTAL

All heterostructures were grown on 100 mm diameter p-doped ($0.5\text{--}0.75\ \Omega\text{ cm}$) Si(111)-wafers. Prior to layer growth in a DCA S1000 molecular beam epitaxy (MBE) cluster system, the samples underwent *ex situ* cleaning by a UV/ozone treatment coupled with a diluted HF etch step (0.2%). The deposition chamber of the MBE multi-chamber system reaches a base pressure of 1.3×10^{-10} mbar. Ge, Si, and granular Nd_2O_3 were evaporated by electron beams and carbon was sublimated from a pyrolytic graphite filament in a SuKo-65 from Dr. Eberl MBE-Komponenten. To maintain a stable oxygen partial pressure, pure oxygen (6N purity) was introduced using a piezo leakage valve. The growth process was monitored *in situ* through reflection high-energy electron diffraction (RHEED) using a RHEED 35 from STAIB Instruments, which allows for real-time observation of the surface reconstruction and layer morphology during growth.

Analysis of the samples was carried out *in vacuo* in a separate chamber of the multi-chamber system. X-ray photoelectron spectroscopy (XPS) was performed using a Mg-Al double anode XR 50 source and a Phoibos 1000 concentric hemispherical analyzer equipped with a fivefold channeltron from SPECS. Both the source and detector are set at a fixed angle of 55.4° . To assess the crystallinity, lattice constants, crystal phase of the oxide layer, composition of the virtual substrate, and degree of relaxation of each layer, x-ray diffraction (XRD) measurements were conducted with a Bruker AXS D8 Discover II diffractometer. We analyzed the cubic phase of the virtual substrates regarding lattice constants, composition, and degree of relaxation by XRD in skew geometry according to Zaumseil.^{35,36} This method was also applied to examine the strain of the cubic phase of the oxide layers. The surface roughness of the samples was determined via atomic force microscopy (AFM) with a Park Scientific Autoprobe M5 in a contact mode. Further investigations included transmission electron microscopy (TEM) operating a FEI Tecnaï G2 F20 operated at 200 kV. Energy

dispersive x-ray spectroscopy (EDS) was done using TEM FEI Tecnaï Osiris operated in a scanning mode at 200 kV.

Following the *ex situ* cleaning of the samples, *in situ* thermal preparation was performed at 750°C , confirming a 7×7 surface reconstruction. Subsequently, virtual $\text{Si}_{1-x}\text{Ge}_x$ substrates were grown via carbon-mediated epitaxy, as described in our previous works.^{37–40} The virtual substrates exhibit a Ge content of $0.55 < x \leq 1$ and a C coverage of 0.4 ML which works as a surfactant.

Nd_2O_3 growth was carried out with an oxygen partial pressure of 6.3×10^{-7} mbar. The growth temperature was adjusted based on the underlying material, virtual substrate or Si substrate. In the case of growth directly on Si(111), the sample was cooled to 650°C following thermal preparation, and Nd_2O_3 was evaporated with an oxygen partial pressure of 6.3×10^{-7} mbar as described by Wang *et al.*⁴¹ However, when Gd_2O_3 was grown on virtual Ge substrates with this growth process, islanding occurred, necessitating a modification of the growth temperature.⁴² According to these results, the germanium-rich $\text{Si}_{1-x}\text{Ge}_x$ layers were heated to 400°C after virtual substrate growth at 150°C . At this temperature, Nd_2O_3 was evaporated while the substrate temperature was increased to 650°C with a ramp of $100\ \frac{\text{K}}{\text{min}}$, and again the oxygen partial pressure was adjusted to 6.3×10^{-7} mbar. Finally, an amorphous Si cap layer was deposited to protect the oxide layer.

III. RESULTS

A. RHEED

After growth of the Ge-rich $\text{Si}_{1-x}\text{Ge}_x$ layers as virtual substrates, the *in situ* RHEED control shows a smooth surface with all layers displaying a $c(2 \times 8)$ surface reconstruction.³⁹ Subsequent annealing to 400°C results in a 7×7 surface reconstruction for a Ge content of $0.55 < x < 1$. Ge layers exhibit a $c(2 \times 8)$ reconstruction just before transitioning to a 1×1 reconstruction, as described in Ref. 40. This transition is indicated by the weakening of the intensity of the sub streaks. The Si surface shows a 7×7 surface reconstruction as expected after thermal preparation. The RHEED patterns before oxide growth are depicted in Fig. 1 on the left-hand side, while patterns after oxide growth are presented on the right-hand side for one representative sample from each substrate. The streaky patterns indicate a smooth surface, which is confirmed by AFM measurements revealing a root-mean-square surface roughness below 0.6 nm for all samples.

After Nd_2O_3 growth, the RHEED patterns differ from each other for growth directly on Si(111) and growth on the virtual substrates. We observe three additional sub streaks when grown on virtual substrates while no sub streaks are observed after growth on Si. The three additional sub streaks could be explained similarly to growth of Gd_2O_3 , where these streaks indicated a crystalline cubic surface structure.²⁷ Due to its similarity to cubic Nd_2O_3 , we infer that our observed RHEED patterns of oxide layers grown on Ge-rich SiGe indicate a cubic Nd_2O_3 surface structure. However, the RHEED pattern after growth on Si(111) differs from the patterns observed by Wang *et al.*,⁴¹ indicating a different surface structure.

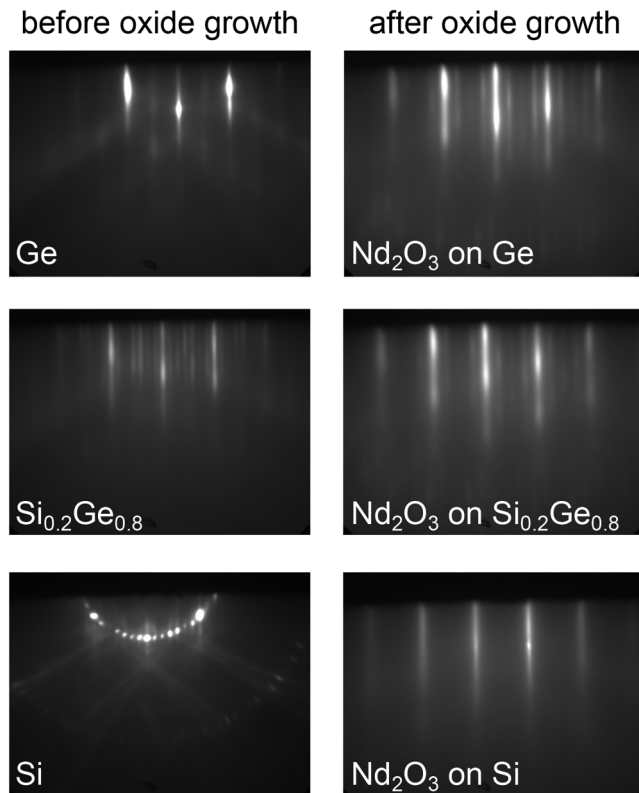


FIG. 1. *In situ* RHEED control of three exemplary samples before and after oxide growth in the $\langle 1\bar{1}0 \rangle$ direction. Before oxide growth, the Si(111) and SiGe surface exhibit a 7×7 surface reconstruction, while the Ge layer shows a $c(2 \times 8)$ reconstruction. After oxide growth, the RHEED pattern of the oxide grown on Ge and SiGe shows three additional subspots, while the oxide layer grown directly on Si shows no subspots.

B. XRD

We conducted an in-depth analysis of the crystallographic phase of the Nd_2O_3 layers using XRD measurements. The results of our symmetrical $\theta/2\theta$ measurements are shown in Fig. 2. Notably, the Nd_2O_3 layer grown directly on Si(111) exhibits a hexagonal structure while growth on Ge results in a cubic structure. Oxide layers grown on SiGe show a mixed phase containing both cubic and hexagonal parts, regardless of their layer thickness. Furthermore, it is evident that the oxide layers grown on Ge exhibit strong tensile strain, while the hexagonal phase grown on Si(111) shows no indication of strain. Growth on SiGe results in relaxation of tensile strain in the cubic phase, even at very high Ge contents of $x > 0.9$.

To delve deeper into the strain analysis of the cubic phase, we performed XRD measurements in the skew geometry, a method described in more detail elsewhere.^{35,36,39} Due to the A/B stacking of cubic REOs on (111)-oriented Si and Ge,^{35,43–45} skew geometry facilitates examination of the virtual Ge substrate and oxide layer without overlapping diffraction peaks. The results are presented in

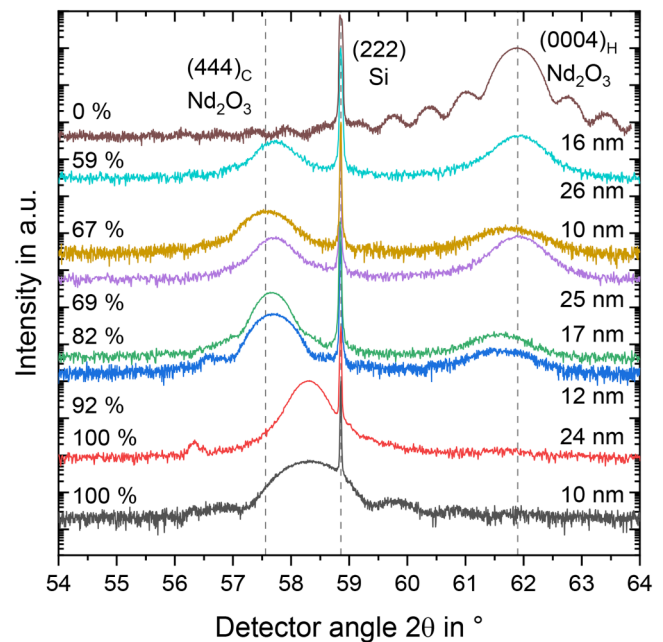


FIG. 2. Results of symmetrical $\theta/2\theta$ measurements with XRD for exemplary samples with varying oxide thickness as indicated on the right-hand side and Ge content of the virtual substrate as written on the left-hand side. For reference, we marked the positions of the diffraction peaks of the (444) and (0004) planes of Nd_2O_3 and the Si substrate (222) peak. At the top, a Nd_2O_3 layer on Si(111) is shown and the Ge content in the virtual substrate increases from top (Si) to bottom (Ge). Nd_2O_3 layers grown on Si exhibit the hexagonal phase, while growth on Ge results in the cubic phase. The Nd_2O_3 layers on SiGe show peaks for both phases.

22 March 2024 06:55:37

Fig. 3 for various oxide layers grown on virtual SiGe substrates. For clarity, we show oxide layers grown on pure Ge with different layer thicknesses in Fig. 3(a) and oxide layers grown on various $\text{Si}_{1-x}\text{Ge}_x$ layers in Fig. 3(b). In these plots, the lattice constant a_{hkl} of the corresponding lattice planes indicated is displayed as a function of $\cos^2(\chi)$, where χ is defined as the angle between the out-of-plane direction and the examined lattice planes. The linear interpolation of a_{hkl} allows the determination of the in-plane and out-of-plane lattice constant of a cubic system, thus facilitating the calculation of strain.

Figure 3(a) reveals fully relaxed virtual Ge substrates, while the oxide layers exhibit substantial tensile strain, regardless of the layer thickness. In contrast, the results for oxide layers grown on SiGe, as shown in Fig. 3(b), indicate almost fully relaxed oxide layers, with the virtual substrates also remaining in a fully relaxed state.

We further determine the epitaxial relation of the oxide layer and virtual substrate by performing XRD measurements in grazing incidence. These results indicate an epitaxial relation of $\text{Nd}_2\text{O}_3(0001)[2\bar{1}\bar{1}0] \parallel \text{SiGe}(111)[1\bar{1}0]$ for the hexagonal phase and the A/B stacking for the cubic phase is confirmed, corresponding to a relation of $\text{Nd}_2\text{O}_3(111)[\bar{1}10] \parallel \text{SiGe}(111)[1\bar{1}0]$. These epitaxial

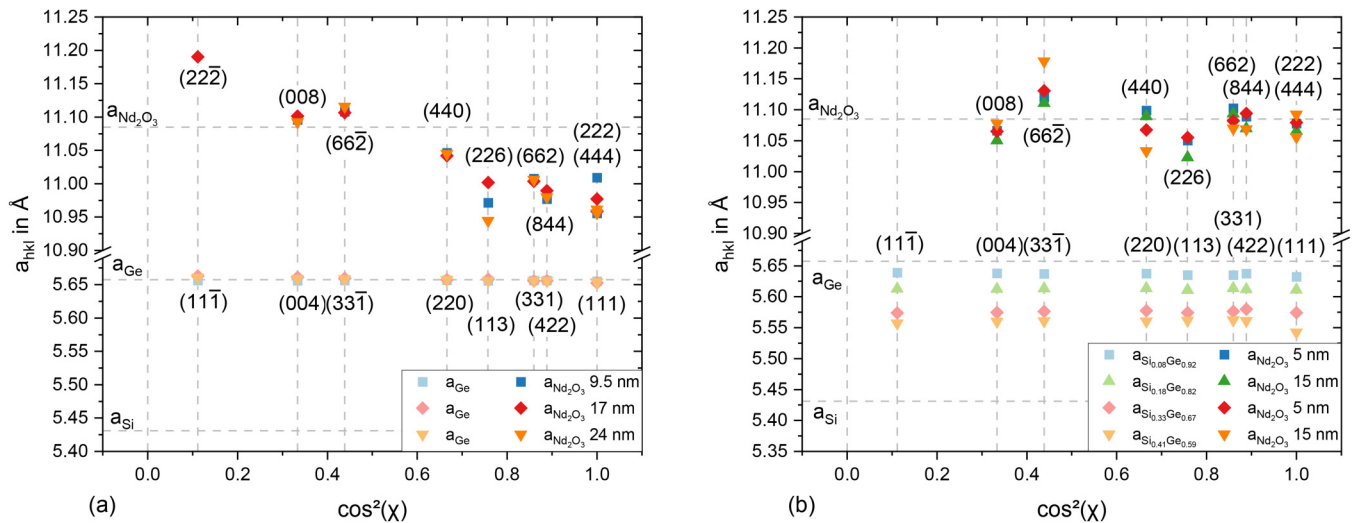


FIG. 3. Analysis of exemplary samples with XRD in the skew geometry. The determined lattice constants a_{hkl} as a function of $\cos^2(\chi)$ are shown and the examined lattice planes (hkl) are indicated. Furthermore, the bulk values for Si, Ge, and Nd_2O_3 are added for reference. For clarity, we show different oxide layer thicknesses on Ge in (a) and various samples with varying Ge content and oxide thickness in (b). The symbols stand for one sample in each plot while the lighter color of each shows the virtual substrate and the saturated color displays the results of the oxide layers. All virtual substrates are fully relaxed, while the linear interpolation of the cubic oxides grown on Ge in (a) exhibits a negative slope indicating tensile strain. The cubic phase of the oxides grown on SiGe seems to be relaxed.

relations are consistent with the hexagonal oxide layer on Si(111) and the cubic phase on Ge. Additionally, we compare the intensities of the diffraction peaks of the cubic and hexagonal phases and see an increase in the hexagonal-to-cubic ratio of the oxide layer with increasing oxide layer thickness and decreasing Ge content when grown on SiGe.

C. XPS

To investigate the bonding configuration and its relationship with the hexagonal phase of the oxide layer, we also performed an *in vacuo* XPS analysis using the Al K_{α} line (1486.6 eV). Specifically, we measured the Ge3d and Si2p peaks before and after approximately 1.5 nm of oxide growth. The results of an exemplary $Si_{0.18}Ge_{0.82}$ layer are presented in Fig. 4. The blue line represents measurements at the SiGe surface, while the red line was measured at the interface.

We establish peak models using Casa XPS.⁴⁶ For the spin-orbit components, Si2p_{1/2} and Si2p_{3/2}, we keep the full width at a half maximum almost equal, choose the area ratio according to the spin-orbit splitting, and maintain a distance of around 0.6 eV. The same principle is applied to Ge3d_{5/2} and Ge3d_{3/2}, with a splitting of around 0.57 eV.⁴⁷ A Shirley background is used,^{48,49} averaging the start and end point over various data points. These parameters remain constant across all peak fits.

In Fig. 4(a), the oxidation states of Ge are marked in increasing order with shifts of 0.8, 1.8, 2.7, and 3.3 eV relative to the Ge^0 state of the $Ge3d_{5/2}$ at 29.8 eV.⁵⁰ In these measurements, we only observe the Ge^0 state even after growing approximately 1.5 nm of Nd_2O_3 indicating no bonding of Ge with the oxide layer. Similarly, we indicate the Si oxidation states in Fig. 4(b) with shifts of 0.9,

1.9, 2.6, and 3.4 eV relative to the Si^0 of the Si2p_{3/2} at 99.8 eV.⁵⁰ These figures reveal a reaction in the Si2p peak spectrum after growing approximately 1.5 nm of Nd_2O_3 . A component around the Si^{3+} oxidation state occurs, indicative of silicate-like bonding,^{51,52} while no component near the Si^{4+} state is present, corresponding to SiO_2 formation.

The O1s spectrum after growth of Nd_2O_3 with a thickness of 1.5 nm shows two peaks in Fig. 5. One at 530 eV can be assigned to oxygen in Nd_2O_3 molecules, consistent with values from the literature.⁵³ The second peak, at around 531.3 eV, is too low in binding energy to be attributed to SiO_2 formation, suggesting silicate-like Nd–O–Si bonding.^{51,52} Thus, we infer the presence of silicate-like bonding at the interface.

Our XPS analysis of the interface of oxide growth on Ge shows no reaction of Ge with oxygen. Instead, we observe a shift in the Ge3d peak to lower binding energies, while the O1s spectrum exhibits one peak corresponding to oxygen in Nd_2O_3 molecules. Consequently, we expect that the oxide layer bonds via Nd with the Ge and germanide-like bonding of the oxide on Ge results.

For further analysis of the interface, we calculate the equivalent homogeneous Ge concentration by $X = \frac{I_p/S_p}{\sum_i I_i/S_i}$ with the intensity of a peak I_j and the sensitivity factor S_j . The sensitivity factor includes the attenuation length and the photoionization cross section.⁵⁴ We approximate the attenuation length of the photoelectrons by the electron mean free path and its value and the photoionization cross-section are taken from Tanuma *et al.*⁵⁵ and Scofield,⁵⁶ respectively. These calculations reveal that the surface of the virtual $Si_{0.18}Ge_{0.82}$ substrate exhibits a Ge content of 88%, consistent with enrichment of Ge at the surface of SiGe layers observed

22 March 2024 06:55:37

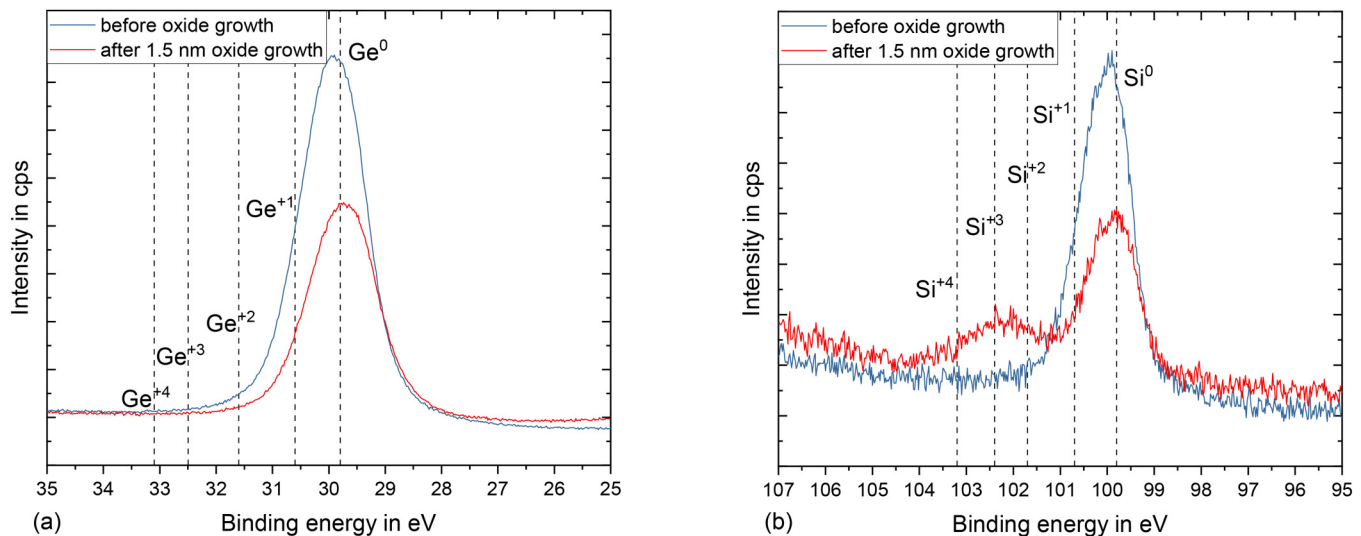


FIG. 4. XPS measurements at the surface of the virtual $\text{Si}_{0.18}\text{Ge}_{0.82}$ substrate (blue lines) and after 1.5 nm oxide growth (red lines) to analyze the interface. We analyzed the Ge3d spectra (a) and the Si2p spectra (b) and marked the different oxidation states in each diagram. In (a), we see no indication of Ge–O bonding after oxide growth, while (b) indicates silicate-like bonding in addition to the Si^0 peak.

before.^{40,57–59} After a 1.5 nm oxide growth, the Ge content at the interface decreased to 86.5%. This decrease further supports the assumption of silicate-like bonding and suggests diffusion of Si toward the interface to form silicate-like bonds.

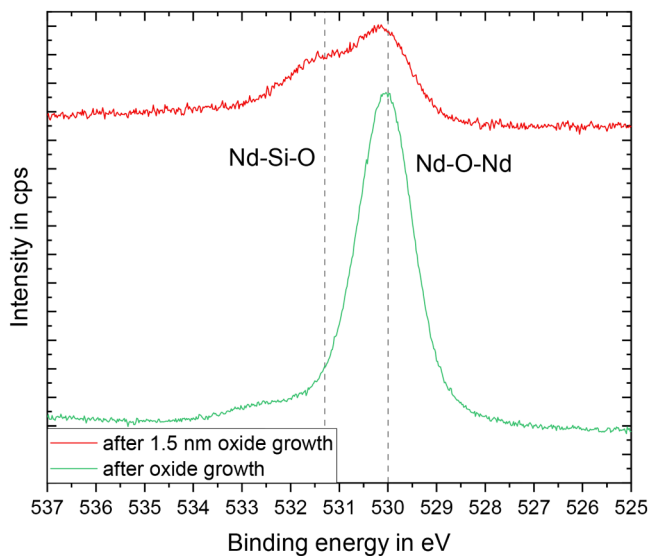


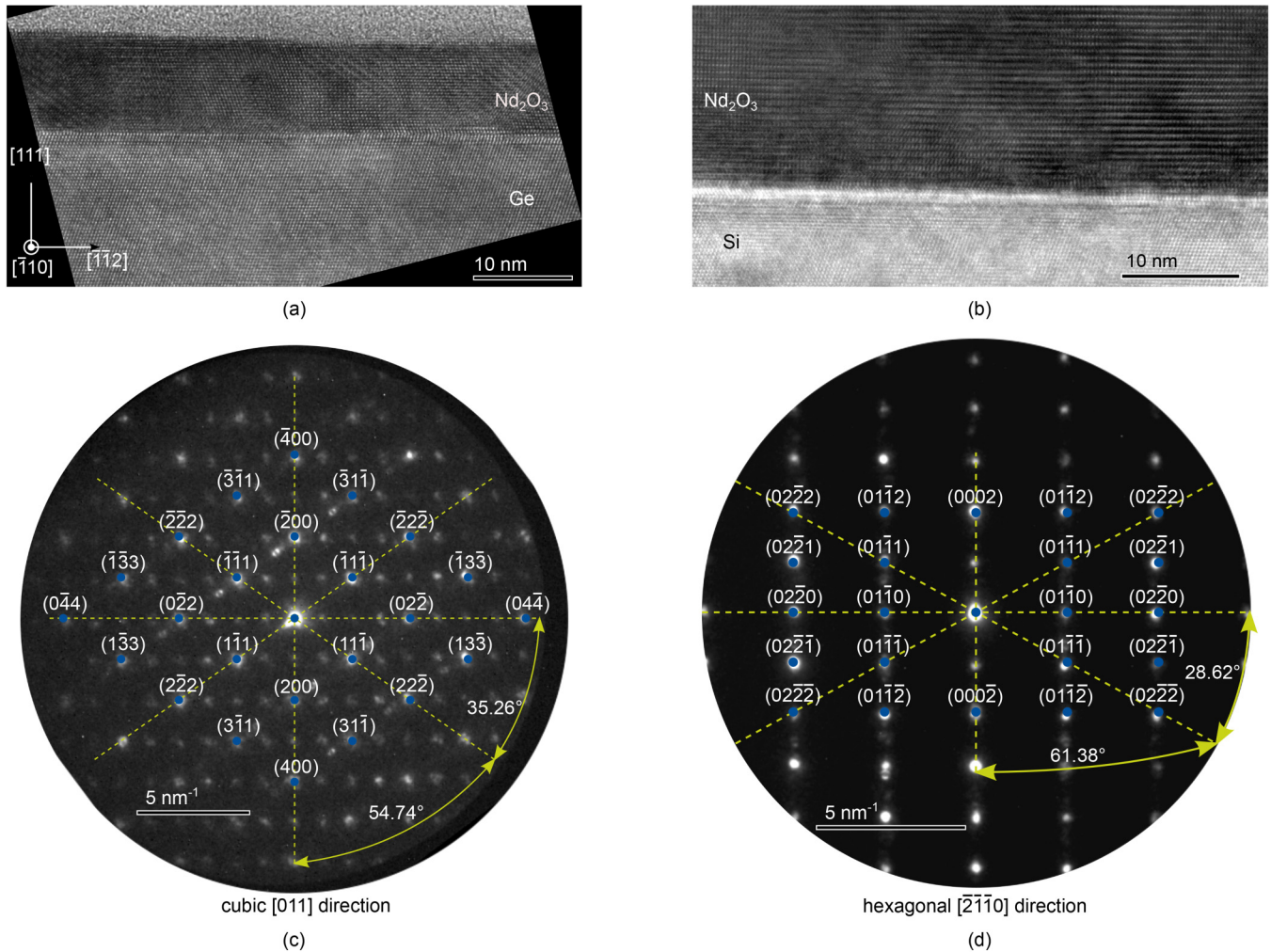
FIG. 5. XPS measurements of the O1s spectrum at the surface after 1.5 nm (red lines) and after 22 nm (green lines) oxide growth. After 1.5 nm oxide growth, two peaks can be fitted at 530 and 531.3 eV which can be assigned to Nd–O–Nd and Nd–O–Si bonding configurations, respectively. After reaching a thickness of 22 nm, only the peak corresponding to Nd–O–Nd bondings in Nd_2O_3 remains.

D. HRTEM/STEM EDS

To get a more profound understanding of the interface processes, we conducted high-resolution TEM (HRTEM). Figure 6 displays cross-sectional HRTEM images of Nd_2O_3 layers grown on Ge and Si. In order to confirm the crystal structure, we obtained by our XRD measurements, we further did a nano beam diffraction study of the oxide layer. Figure 6 shows the diffraction images taken from an oxide layer grown on $\text{Si}_{0.18}\text{Ge}_{0.82}$ at a position of cubic oxide growth (c) and grown directly on Si(111) (d). The theoretical diffraction pattern of a cubic crystal structure in the [011] direction is sketched in (c) and matches the observed diffraction pattern of the oxide. For the oxide layer grown on Si(111) in (d), the diffraction pattern corresponds well with the expected pattern of an hexagonal crystal structure in the $[\bar{2}\bar{1}\bar{1}0]$ direction. These results support the crystal structures we obtained from our XRD analysis. In these systems, we observe well-defined, sharp interfaces with no interfacial layer formation. In contrast, Nd_2O_3 layers grown on $\text{Si}_{1-x}\text{Ge}_x$ layers exhibit an amorphous interfacial layer and its thickness increases as the Ge content decreases. At locations where stacking faults extend to the interface, the interfacial layer penetrates deeper into the virtual substrate as shown exemplarily for oxide growth on a virtual $\text{Si}_{0.32}\text{Ge}_{0.68}$ substrate in Fig. 7.

To gain further insights into this interfacial layer, we conducted STEM combined with EDS. The results from the same sample that was analyzed in detail with XPS are depicted in Fig. 8. Figure 8(a) shows the bright-field image that is analyzed with EDS. The detected elements are visualized with spatial resolution in Figs. 8(c)–8(f). The detected intensities of the relevant elements are presented in Fig. 8(b). To identify specific positions, such as the interface between the oxide layer and the amorphous Si cap layer, as well as the boundaries of the interfacial layer, we marked these areas with numbers 1–3 in all images.

22 March 2024 06:55:37



22 March 2024 06:55:37

FIG. 6. High-resolution TEM images of Nd_2O_3 layers grown on Ge (a) and Si (b). Both samples show a sharp interface and no grain boundaries. We also show nano beam diffraction images taken from an oxide layer grown on $\text{Si}_{0.18}\text{Ge}_{0.82}$ (c) at a position of cubic oxide growth and on Si (d). The diffraction images in (c) and (d) match the theoretical diffraction pattern sketched in blue dots of a cubic phase and hexagonal phase, respectively, as indicated.

For this particular sample, the interfacial layer exhibits a layer thickness of approximately 5.5 nm. Furthermore, this analysis reveals depletion of Si at the interface of the $\text{Si}_{0.18}\text{Ge}_{0.82}$ layer and reaction with the oxide to form a silicate. Based on the literature, mainly two $\text{SiO}_2\text{-Nd}_2\text{O}_3$ configurations are known, namely, Nd_2SiO_5 and $\text{Nd}_2\text{Si}_2\text{O}_7$.^{51,60} Our quantification of the interfacial layer approximately agrees with these two configurations, suggesting the presence of $\text{Nd}_2\text{Si}_2\text{O}_7$ at the interface toward the virtual substrate and Nd_2SiO_5 at the interface with Nd_2O_3 .

IV. DISCUSSION

A. Strain in the oxide

To understand the crystalline phases observed in the Nd_2O_3 layers, it is essential to examine previous research on phase

transitions in REOs. Several studies have explored phase transitions in REOs, particularly Gd_2O_3 , with a focus on factors such as pressure, growth conditions, and stress.^{29–34} For instance, investigations revealed thickness-dependent phase transitions in Gd_2O_3 when grown on different substrates, such as GaN, SiC, and GaAs,^{61–63} with transitions from the hexagonal to the monoclinic phase. When grown on Ge(001), a mixture of the cubic and monoclinic phase was observed.⁶⁴ It was also noted that tensile stress can stabilize cubic Gd_2O_3 , while compressive stress leads to a transition to the monoclinic structure.³⁰ The transition from cubic Gd_2O_3 to the monoclinic and hexagonal phase can be achieved by increasing atmospheric pressure,^{31–33} and thermodynamically, an increase in temperature can also drive such a transition.²⁵ Additionally, low growth temperatures can result in non-cubic growth of REOs like Gd_2O_3 on Si(111),²⁹ and the oxygen chemical potential has been

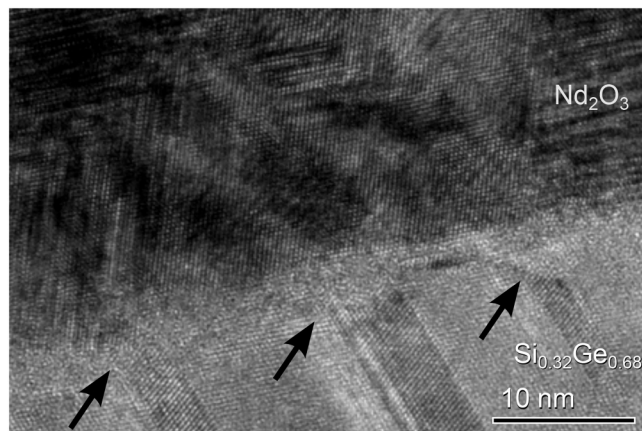


FIG. 7. High-resolution TEM image of a Nd_2O_3 layer grown on a virtual $\text{Si}_{0.32}\text{Ge}_{0.68}$ substrate. An amorphous interfacial layer can be seen that penetrates deeper into the virtual substrate where stacking faults reach the interface as marked by arrows.

found to influence the observed crystalline phase of Gd_2O_3 .^{65,66} A systematic study of Gd_2O_3 growth on $\text{Si}(001)$ revealed a strong influence of both kinetic and thermodynamic factors on the crystal structure.³⁴ At low temperatures around 250°C , the cubic phase was observed, and increasing oxygen partial pressure induced growth of the monoclinic structure, which remained stable even during temperature ramping.

In the case of Nd_2O_3 , a phase transition from cubic to hexagonal appears thermodynamically by an increase in temperature around 600°C ,⁶⁷ although other calculations suggested the presence of only the hexagonal phase.²⁵ Busani *et al.*²⁸ achieved hexagonal Nd_2O_3 at low temperatures of 280°C and slow deposition rates, while the cubic structure was predominant under any other condition. They state that the hexagonal structure is normally only expected after annealing above 850°C .

Given our growth conditions in this study, two possibilities arise: either a stress-induced phase transition or a transition driven by nucleation mechanisms induced by interface reactions.

Initially, we consider a strain-induced phase transition. The cubic Nd_2O_3 phase is well-matched with SiGe layers containing approximately 52%. Consequently, higher Ge content in the virtual

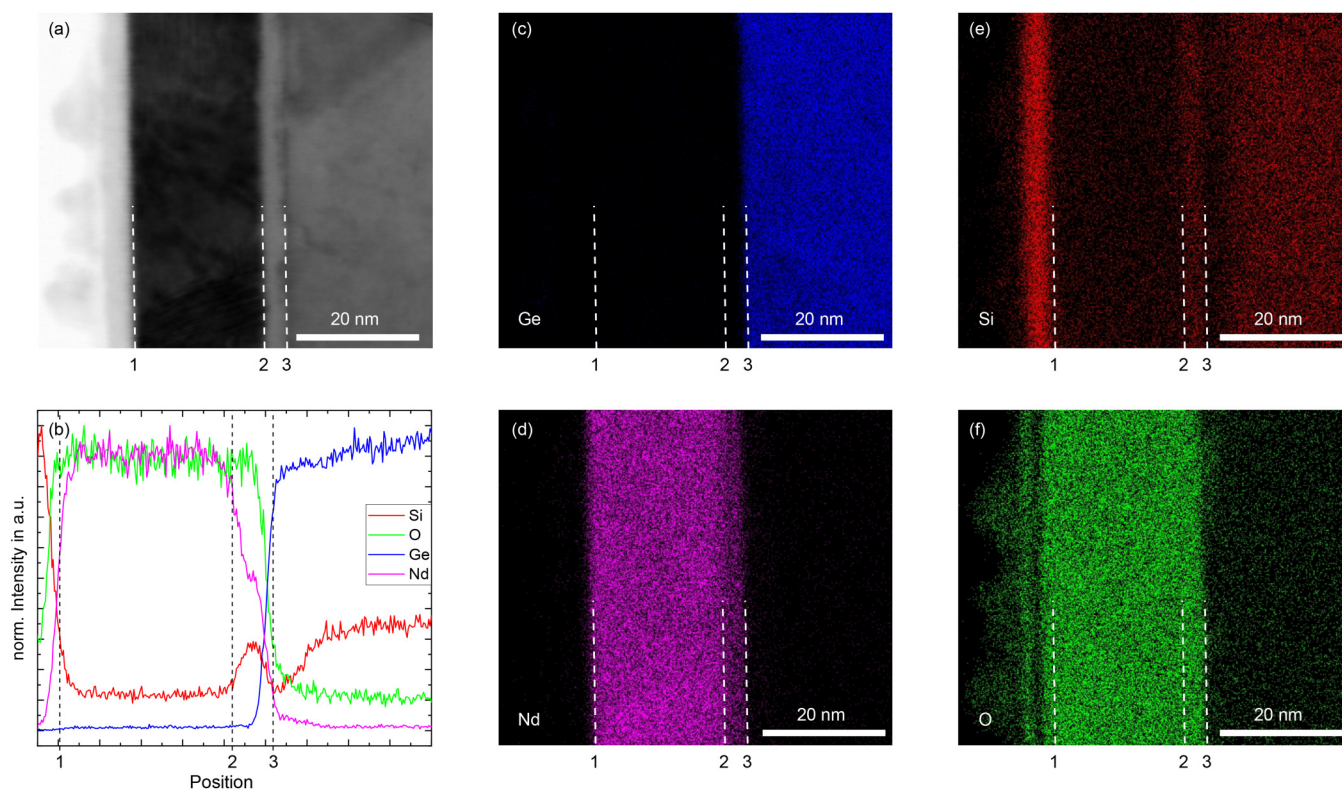


FIG. 8. Results of our STEM-EDS analysis of a 22 nm thick Nd_2O_3 layer on a $\text{Si}_{0.18}\text{Ge}_{0.82}$ layer. On the left-hand side at the top, the bright-field STEM image is shown. In all images, position 1 corresponds to the interface between the oxide layer and the amorphous Si cap layer, while positions 2 and 3 indicate the interfaces of the interfacial layer with the Nd_2O_3 and $\text{Si}_{0.18}\text{Ge}_{0.82}$ layer, respectively. The diagram on the left-hand side at the bottom indicates the measured intensities of Si, O, Ge, and Nd. The corresponding maps for these four elements are shown in the images in the middle and right-hand side. An interfacial layer is visible and shows depletion of Si at the surface of the SiGe layer that diffused to the oxide and reacted to a silicate.

22 March 2024 06:55:37

substrate should induce greater tensile strain in the cubic oxide layer, while increased Si content would result in higher compressive strain. Our XRD results in Fig. 3 show significant tensile strain of around 1% in cubic Nd_2O_3 when grown on Ge, yet the cubic phase of oxide layers appears nearly relaxed with a remaining strain of less than 0.1% when deposited on virtual SiGe substrates with Ge contents above 90%. Even oxide layers on SiGe with a Ge content close to 52% exhibit hexagonal parts, as shown in Fig. 2. These hexagonal parts show increasing strain with increasing Ge content from no strain for Ge contents below 60% up to 0.6% if the SiGe substrate contains above 90% Ge. These results demonstrate that Nd_2O_3 behaves somewhat similarly to Gd_2O_3 , since strong compressive strain leads to the hexagonal phase in the oxide layer when grown directly on Si(111). However, it is worth noting that only the highest level of tensile strain stabilizes the cubic phase in the Nd_2O_3 layer on a Ge layer, while slightly less tensile strain on a virtual $\text{Si}_{0.08}\text{Ge}_{0.92}$ substrate is insufficient to fully stabilize the cubic phase, resulting in the coexistence of hexagonal parts. Because even nearly lattice-matched cubic oxide growth on SiGe exhibits hexagonal characteristics, we can reasonably rule out a strain-induced phase transition as the sole cause of hexagonal oxide growth. However, the hexagonal phase seems to compensate the elastic energy in the oxide layer with increasing Ge content in the virtual substrate while the cubic phase stays nearly relaxed when grown on virtual SiGe substrates.

B. Processes at the interface

At this point it appears like the Si content at the interface plays a crucial role in the growth of oxide layers, as the hexagonal content in the oxide layer increases with increasing Si content in the virtual substrate. While there is a slight increase in the hexagonal-to-cubic ratio concerning increasing oxide layer thickness, the Si content dependency is much more prominent. This suggests that the growth of Nd_2O_3 , like Gd_2O_3 ,³⁴ strongly depends on the initial nucleation processes, which we need to examine further regarding the interface and silicate formation. It is worth noting that no evidence of the amorphous interfacial layer was observed during growth using RHEED, suggesting that the formation of this layer occurs during subsequent growth.

First, we consider the possibility of GeO desorption from the SiGe layer, followed by a reaction of the oxide layer with the remaining Si to form a silicate. Previous research on GeO desorption kinetics has provided insights into this process.^{15,68–71} It was observed that adsorption and interaction of oxygen on a Ge surface leads to desorption of GeO molecules at temperatures as low as 400°C.⁶⁸ In the case of a GeO_2/Ge stack, desorption begins at the bottom interface and is limited by subsequent diffusion through the oxide. Annealing such a GeO_2/Ge stack in ultra-high vacuum (UHV) at 650°C or above leads to desorption and even etching of the underlying Ge substrates.^{70,71} This can be limited by the insertion of a SiO_2 interfacial layer that suppresses reactions with the Ge substrate.^{15,69} Applying these results to our study, we cannot fully rule out GeO desorption in our $\text{Nd}_2\text{O}_3/\text{Ge}$ stacks, as the growth temperature is above 400°C. However, the desorption is diffusion-limited, and a temperature of 650°C is only reached after a certain oxide layer thickness is already established. We also see no reaction

of oxygen with Ge at the interface in our XPS results or degraded interfaces in our TEM results. Thus, we propose GeO desorption is unlikely.

Nevertheless, investigations of the kinetics of GeO desorption during oxidation of SiGe surfaces have yielded different results. Li *et al.*⁷¹ did not observe any GeO desorption that is associated with the reaction of GeO_2 and Ge when they annealed GeO_2/SiGe stacks in UHV up to temperatures of 700°C. Since our growth conditions do not reach such high temperatures, we exclude GeO desorption followed by a reaction of Nd_2O_3 with the remaining Si as the formation mechanism for the interfacial silicate layer.

Understanding the formation of the silicate layer requires consideration of several processes at the interface. The mechanisms of silicate formation for REO growth on Si are influenced by factors like temperature, time, and the ion radius of the rare-earth (RE) element. For example, it has been found that an increase in Si–O–Ln bonds depends on the post-annealing temperature, which, in turn, relies on the ion radius of the RE element.⁷² Given the “lanthanide contraction,” light RE elements like Nd have larger ion radii, making it easier for their metal oxides to form silicate layers.

Early investigations suggested Si diffusion from the substrate into the RE oxide, followed by a reaction, as the primary process for silicate layer formation.^{52,73–76} However, subsequent research revealed that annealing of capped Si/REO structures prevents silicate formation, promoting a different mechanism where diffused oxygen reacts with the Si substrate, resulting in Si–O molecule diffusion and reaction with the REO to form silicates.^{72,77,78} The cubic structure of REO is inherently defective, with one-fourth of the sites in the anion sublattice remaining unoccupied. Thus, this structure exhibits relatively unimpeded pathways along the (111) directions for the migration of oxygen through the lattice.⁷⁹

Silicate formation is only observed for samples with Nd_2O_3 grown on SiGe that exhibit a mixed phase where the cubic phase is involved. Thus, we expect the incorporation of additional supplied oxygen at the growing Nd_2O_3 surface via oxygen vacancy annihilation. The large diffusion coefficient and low activation energy of atomic oxygen in cubic REOs allow for a high enough oxygen flux to arrive at the interface to react with Si.^{77,79} The single-crystal hexagonal phase exhibits no inherent oxygen vacancies in its crystal symmetry and, therefore, lacks such pathways for oxygen diffusion, leading to a low oxygen flux at the interface that might be insufficient for silicate formation when grown on Si(111).

However, the surface of the grown SiGe layers is highly enriched with Ge. For Si to react with oxygen, further diffusion processes are required. Several studies on the oxidation of SiGe layers with Ge contents mainly below 50% showed formation of SiO_2 on top of a Ge-rich layer,^{80,81} whereas oxidation of SiGe layers with higher Ge contents results in mixed oxide growth.^{81–83} This oxidation behavior of SiGe layers depends on several parameters like Ge content of the layer, oxidation temperature, oxygen partial pressure meaning oxygen chemical potential at the growing interface, strain, and layer thickness.^{82,84} For a given set of growth parameters, it is assumed that for high Si contents only Si is oxidized initially, with Ge left behind piling up at the interface to form a Ge-rich layer. Subsequently, more Si diffuses through this Ge-rich layer to react with oxygen arriving at the interface after diffusing through the growing oxide layer. If the Si concentration is

too low or the oxygen concentration at the interface is too high for selective Si oxidation, Ge and Si oxidize simultaneously, resulting in mixed oxide growth.⁸¹ As long as Si is present during Ge oxidation, GeO_2 is reduced by Si to SiO_2 due to the difference in Gibbs free energy, leading to Ge atoms piling up at the interface.^{1,80,82,85} A crucial parameter for controlling the interface during SiGe oxidation is the effective oxygen pressure at the interface.^{86,87} A high oxygen chemical potential at the interface combined with a low temperature result in mixed oxide growth, whereas higher temperatures with a lower oxygen chemical potential favor selective Si oxidation.^{71,87,88} The low temperature results in low Si diffusivity, while the high oxygen partial pressure increases arriving oxygen amount at the interface, leading to Ge oxidation.¹ According to those results, a temperature of 650°C and an oxygen partial pressure in the range of 10^{-7} mbar should be in the preferential regime for SiO_2 formation.⁸⁷ Additionally, selective Si oxidation has been demonstrated on $\text{Si}_{0.16}\text{Ge}_{0.84}$ at a temperature of 600°C with a partial pressure of 0.01 Torr.¹¹

Selective oxidation of Si strongly depends on Si diffusion from the SiGe layer to the oxidizing interface. This diffusion is also affected by defect generation at the interface, which is quite different compared to the Si/ SiO_2 interface. Interstitial emission from the oxidizing interface is still present but relatively small compared to the Si oxidation. The Si diffusion flux rather creates a vacancy excess, which can account for further Si diffusion upon inward diffusion. Furthermore, the vacancy flux can recombine with most of the Ge interstitials emitted from the oxidizing interface.^{80,89} The temperature dependence of Si and Ge diffusion in a SiGe alloy follows the Arrhenius expression, allowing for the calculation of the diffusion coefficient $D = D_0 \exp(-E_a/k_B T)$ with the preexponential factor D_0 , the activation enthalpy E_a , the Boltzmann constant k_B , and the temperature T .^{90,91} It was found that the activation enthalpy decreases for Si and Ge diffusion in SiGe with increasing Ge content, suggesting that both Si and Ge diffuse via a vacancy mechanism in SiGe alloys with a Ge content above 30%,^{90,92} which agrees with the observed defect generation at an oxidizing SiGe interface. Using the calculated diffusion coefficient, we can then estimate the diffusion length X of Si in a given SiGe alloy over a given time t by $X = \sqrt{Dt}$.⁹²

The sample analyzed in STEM-EDS in Fig. 8 shows a Ge pile-up, meaning the region depleted from Si reaching from position 3 deeper into the virtual substrate, with a thickness of approximately 5.5 nm. From XPS we get a surface-near Ge content of 88%, while XRD measurements result in a bulk Ge content of 82%. We estimate the diffusion coefficient of Si in SiGe by linear interpolation of D_0 and E_a taken from Kube *et al.*⁹¹ For the surface-near Ge-content, the calculated values are $D_{0,x=0.88} = 171.6^{+116.8}_{-64.8} \text{ cm}^2/\text{s}$ and $E_{a,x=0.88} = 3.61 \pm 0.2 \text{ eV}$, which leads to a Si diffusion length of $X_{x=0.88} = 1.5^{+3}_{-1} \text{ nm}$ for our temperature of 650°C and the growth time of 2 h. For the bulk value of $x = 0.82$ the diffusion length decreases rapidly and we can calculate accordingly a diffusion length of $X_{x=0.82} = 0.7^{+1}_{-0.5} \text{ nm}$. This shows the strong dependence of Si diffusion on the Ge content. Since XPS estimates the Ge content with the assumption of a homogeneous material, the Ge content at the surface is expected to be even higher and increases even further during the reaction of the diffused Si with arriving oxygen leading to a larger diffusion length than we estimate here.

From this, we conclude that the additional oxygen partial pressure leads to oxygen diffusion through the growing oxide layer. The growth temperature and oxygen partial pressure are in the region of selective Si oxidation.⁸⁷ Thus, oxygen arriving at the interface reacts with Si, similar to SiGe surface oxidation, resulting in Si diffusion toward the interface and the formation of a Ge pile-up. The Si-O molecules then react with the Nd_2O_3 layer, forming an interfacial silicate layer. The thickness and composition of this silicate layer are constrained by the diffusion length and Si content in the underlying SiGe layer. Since Si is expected to diffuse easily along defects, Si diffusion at stacking faults is increased, leading to locally thicker silicate layers penetrating deeper into the SiGe layer.

Another limiting factor may involve reactions similar to those observed in Pr-silicate reactions.⁹³ Oxygen might not only stem from diffusing oxygen but also to some extent from reduction of Nd_2O_3 moieties. However, the energy gain from this reduction becomes less favorable as the distance from interface increases, as indicated by the estimated Gibbs free formation energy, which is higher for the SiO_2 -rich phase.⁹⁴

The silicate-like bonding seems to be crucial for the emergence of the hexagonal phase. On pure Ge, we observe germanide-like bonding leading to cubic oxide growth while the diffusion of Si and reaction with the oxide on SiGe might be crucial for the emergence of the hexagonal phase. Next to the emergence of silicate-like bonding in order to form the hexagonal phase, the initial surface reconstruction of the virtual substrate might influence the nucleation process and thus the crystal phase of the oxide. Samples exhibiting hexagonal regions in the oxide layer showed a 7×7 surface reconstruction prior to oxide growth, while purely cubic oxide layers were grown on surfaces with a $c(2 \times 8)$ surface reconstruction. The surface reconstructions could, on the one hand, influence the preferred symmetry of nucleation with the 7×7 preferring hexagonal symmetry. On the other hand, the 7×7 reconstruction indicates compressive strain on the surface, while the $c(2 \times 8)$ reconstruction on the verge to transitioning to 1×1 can be observed at tensile strain.^{40,95} As discussed, tensile strain should stabilize the cubic phase, while compressive strain induces a phase transition to the hexagonal phase. The silicate-like bonding in combination with this surface reconstruction and initial surface stress could therefore lead to a preference of the hexagonal phase formation.

V. CONCLUSIONS

In summary, our study of Nd_2O_3 growth on virtual germanium-rich $\text{Si}_{1-x}\text{Ge}_x$ substrates with a Ge content of $0.55 < x \leq 1$ and Si(111) has revealed insights into the dependence of crystalline phases and interface processes of the oxide layers on various substrates. Our analysis showed that Nd_2O_3 grown directly on Si(111) exhibits a hexagonal structure, while growth on Ge leads to a cubic structure. On $\text{Si}_{1-x}\text{Ge}_x$ substrates, a mixed phase of cubic and hexagonal parts is observed, regardless of the Ge content. Oxide layers grown on Ge exhibit strong tensile strain, while layers with hexagonal parts show no strain. XPS combined with TEM and EDS analysis indicate the formation of an interfacial silicate layer on SiGe substrates, which increases in thickness as the Ge

content decreases. We attribute the silicate formation to the high diffusion rate of oxygen through cubic Nd_2O_3 , as well as Si diffusion toward the interface with the virtual substrate. The emergence of the hexagonal phase in the oxide layers might be influenced by the surface reconstruction of the substrate. Samples with hexagonal oxide regions show a 7×7 surface reconstruction before oxide growth, while purely cubic oxide layers are grown on surfaces with a (2×8) surface reconstruction. In conclusion, our investigation highlights the interplay of strain, diffusion processes, and substrate surface reconstruction in the growth of Nd_2O_3 on silicon-based substrates. It provides valuable information on structural properties and silicate formation mechanisms, although the exact mechanisms of the hexagonal phase's emergence require further study.

AUTHOR DECLARATIONS

Conflict of Interest

The authors have no conflicts to disclose.

Author Contributions

H. Genath: Conceptualization (lead); Data curation (lead); Investigation (lead); Methodology (lead); Validation (lead); Visualization (lead); Writing – original draft (lead). **M. A. Schubert:** Data curation (equal); Investigation (equal); Methodology (equal); Writing – review & editing (equal). **H. L. Yamtomo:** Data curation (equal); Investigation (equal); Writing – review & editing (equal). **J. Krügener:** Methodology (supporting); Project administration (equal); Resources (equal); Supervision (equal); Writing – review & editing (equal). **H. J. Osten:** Project administration (equal); Supervision (equal); Writing – review & editing (equal).

DATA AVAILABILITY

The data that support the findings of this study are available from the corresponding author upon reasonable request.

REFERENCES

- ¹E. Long, A. Azarov, F. Kløw, A. Galeckas, A. Yu Kuznetsov, and S. Diplas, “Ge redistribution in SiO_2/SiGe structures under thermal oxidation: Dynamics and predictions,” *J. Appl. Phys.* **111**, 024308 (2012).
- ²D. K. Nayak, J. C. S. Woo, J. S. Park, K. L. Wang, and K. P. MacWilliams, “High-mobility *p*-channel metal–oxide–semiconductor field-effect transistor on strained Si,” *Appl. Phys. Lett.* **62**, 2853–2855 (1993).
- ³K. Sawano, Y. Abe, H. Satoh, Y. Shiraki, and K. Nakagawa, “Compressive strain dependence of hole mobility in strained Ge channels,” *Appl. Phys. Lett.* **87**, 192102 (2005).
- ⁴J. Mitard, B. de Jaeger, G. Eneman, A. Dobbie, M. Myronov, M. Kobayashi, J. Geypen, H. Bender, B. Vincent, R. Krom, J. Franco, G. Winderickx, E. Vrancken, W. Vanherle, W.-E. Wang, J. Tseng, R. Loo, K. de Meyer, M. Caymax, L. Pantisano, D. R. Leadley, M. Meuris, P. P. Absil, S. Biesemans, and T. Hoffmann, “High hole mobility in 65 nm strained Ge *p*-channel field effect transistors with HfO_2 gate dielectric,” *Jpn. J. Appl. Phys.* **50**, 04DC17 (2011).
- ⁵T. David, A. Benkouider, J.-N. Aqua, M. Cabie, L. Favre, T. Neisius, M. Abbarchi, M. Naffouti, A. Ronda, K. Liu, and I. Berbezier, “Kinetics and energetics of Ge condensation in SiGe oxidation,” *J. Phys. Chem. C* **119**, 24606–24613 (2015).

- ⁶A. Nanwani, R. S. Pokharia, J. Schmidt, H. J. Osten, and S. Mahapatra, “Improvement of crystal quality and surface morphology of $\text{Ge}/\text{Gd}_2\text{O}_3/\text{Si}(111)$ epitaxial layers by cyclic annealing and regrowth,” *J. Phys. D: Appl. Phys.* **55**, 115302 (2022).
- ⁷S. Paleari, S. Baldovino, A. Molle, and M. Fanciulli, “Evidence of trigonal dangling bonds at the $\text{Ge}(111)/\text{oxide}$ interface by electrically detected magnetic resonance,” *Phys. Rev. Lett.* **110**, 206101 (2013).
- ⁸E. Simoen, J. Mitard, G. Hellings, G. Eneman, B. D. Jaeger, L. Witters, B. Vincent, R. Loo, A. Delabie, S. Sioncke, M. Caymax, and C. Claeys, “Challenges and opportunities in advanced Ge pMOSFETs,” *Mater. Sci. Semicond. Process.* **15**, 588–600 (2012).
- ⁹A. Toriumi and T. Nishimura, “Germanium CMOS potential from material and process perspectives: Be more positive about germanium,” *Jpn. J. Appl. Phys.* **57**, 010101 (2018).
- ¹⁰I. Z. Mitrovic, M. Althobaiti, A. D. Weerakkody, V. R. Dhanak, W. M. Linhart, T. D. Veal, N. Sedghi, S. Hall, P. R. Chalker, D. Tsoutsou, and A. Dimoulas, “Ge interface engineering using ultra-thin La_2O_3 and Y_2O_3 films: A study into the effect of deposition temperature,” *J. Appl. Phys.* **115**, 114102 (2014).
- ¹¹W.-L. Lee, J.-L. Zhang, M.-L. Tsai, S.-Y. Wang, G.-L. Luo, and C.-H. Chien, “Study of high-Ge-content $\text{Si}_{0.16}\text{Ge}_{0.84}$ gate stack by low pressure oxidation,” *ECS J. Solid State Sci. Technol.* **7**, P73–P76 (2018).
- ¹²C. G. van de Walle, M. Choi, J. R. Weber, J. L. Lyons, and A. Janotti, “Defects at Ge/oxide and III–V/oxide interfaces,” *Microelectron. Eng.* **109**, 211–215 (2013).
- ¹³A. Ohta, T. Fujioka, H. Murakami, S. Higashi, and S. Miyazaki, “X-ray photoelectron spectroscopy study of interfacial reactions between metal and ultrathin Ge oxide,” *Jpn. J. Appl. Phys.* **50**, 10PE01 (2011).
- ¹⁴M. S. Kavrik, P. Ercius, J. Cheung, K. Tang, Q. Wang, B. Fruhberger, M. Kim, Y. Taur, P. C. McIntyre, and A. C. Kummel, “Engineering high-*k*/SiGe interface with ALD oxide for selective GeO_x reduction,” *ACS Appl. Mater. Interfaces* **11**, 15111–15121 (2019).
- ¹⁵K. Kita, S. K. Wang, M. Yoshida, C. H. Lee, K. Nagashio, T. Nishimura, and A. Toriumi, “Comprehensive study of GeO_2 oxidation, GeO desorption and GeO_2 -metal interaction—Understanding of Ge processing kinetics for perfect interface control,” in *2009 IEEE International Electron Devices Meeting (IEDM)* (IEEE, 2009), pp. 1–4.
- ¹⁶Y. Oshima, Y. Sun, D. Kuzum, T. Sugawara, K. C. Saraswat, P. Pianetta, and P. C. McIntyre, “Chemical bonding, interfaces, and defects in hafnium oxide/germanium oxynitride gate stacks on $\text{Ge}(100)$,” *J. Electrochem. Soc.* **155**, G304 (2008).
- ¹⁷T. Sasada, Y. Nakakita, M. Takenaka, and S. Takagi, “Surface orientation dependence of interface properties of GeO_2/Ge metal-oxide-semiconductor structures fabricated by thermal oxidation,” *J. Appl. Phys.* **106**, 073716 (2009).
- ¹⁸D. Kuzum, A. J. Pethe, T. Krishnamohan, and K. C. Saraswat, “Ge (100) and (111) N- and P-FETs with high mobility and low-*T* mobility characterization,” *IEEE Trans. Electron Devices* **56**, 648–655 (2009).
- ¹⁹T. Nishimura, C. H. Lee, T. Tabata, S. K. Wang, K. Nagashio, K. Kita, and A. Toriumi, “High-electron-mobility Ge n-channel metal–oxide–semiconductor field-effect transistors with high-pressure oxidized Y_2O_3 ,” *Appl. Phys. Express* **4**, 064201 (2011).
- ²⁰H. van Nguyen, A. Dobbie, M. Myronov, D. J. Norris, T. Walther, and D. R. Leadley, “Epitaxial growth of relaxed germanium layers by reduced pressure chemical vapour deposition on (110) and (111) silicon substrates,” *Thin Solid Films* **520**, 3222–3226 (2012).
- ²¹S. Maikap, M. H. Lee, S. T. Chang, and C. W. Liu, “Characteristics of strained-germanium *p*- and *n*-channel field effect transistors on a Si (111) substrate,” *Semicond. Sci. Technol.* **22**, 342–347 (2007).
- ²²T. Krishnamohan and K. Saraswat, “High mobility Ge and III–V materials and novel device structures for high performance nanoscale MOSFETs,” in *ESSDERC 2008—38th European Solid-State Device Research Conference* (IEEE, 2008), pp. 38–46.
- ²³E. K. Evangelou, G. Mavrou, A. Dimoulas, and N. Konofaos, “Rare earth oxides as high-*k* dielectrics for Ge based MOS devices: An electrical study of $\text{Pt}/\text{Gd}_2\text{O}_3/\text{Ge}$ capacitors,” *Solid-State Electron.* **51**, 164–169 (2007).

- ²⁴A. Dimoulas, "Rare earth oxides grown by molecular beam epitaxy for ultimate scaling," in *Topics in Applied Physics* (Springer, 2007), Vol. 106, pp. 379–390.
- ²⁵M. Zinkevich, "Thermodynamics of rare earth sesquioxides," *Prog. Mater. Sci.* **52**, 597–647 (2007).
- ²⁶M. Foex and J.-P. Traverse, "Remarques sur les Transformations Cristallines Présentées a Haute Température par les Sesquioxydes de Terres Rares," *Rev. Int. Hautes Temp. Refract.* **3**, 429–453 (1966).
- ²⁷J. X. Wang, A. Laha, A. Fissel, D. Schwendt, R. Dargis, T. Watahiki, R. Shayduk, W. Braun, T. M. Liu, and H. J. Osten, "Crystal structure and strain state of molecular beam epitaxial grown Gd₂O₃ on Si(111) substrates: A diffraction study," *Semicond. Sci. Technol.* **24**, 045021 (2009).
- ²⁸T. Busani, R. Devine, and P. Gonon, "Structural effects in the dielectric constant of rare-earth oxides: Nd₂O₃," *ECS Trans.* **1**, 331–340 (2006).
- ²⁹M. Moellers, C. Margenfeld, T. F. Wietler, and H. J. Osten, "Growth of epitaxially stabilized, non-cubic Gd₂O₃ on silicon(111) substrates," *J. Cryst. Growth* **480**, 141–144 (2017).
- ³⁰D. A. Grave, M. P. Schmitt, J. A. Robinson, and D. E. Wolfe, "Stress induced phase transition in Gd₂O₃ films by ion beam assisted reactive electron beam-physical vapor deposition (EB-PVD)," *Surf. Coat. Technol.* **242**, 68–73 (2014).
- ³¹F. X. Zhang, M. Lang, J. W. Wang, U. Becker, and R. C. Ewing, "Structural phase transitions of cubic Gd₂O₃ at high pressures," *Phys. Rev. B* **78**, 064114 (2008).
- ³²F. Manjón, J. Sans, J. Ibáñez, and A. Pereira, "Pressure-induced phase transitions in sesquioxides," *Crystals* **9**, 630 (2019).
- ³³L. Bai, J. Liu, X. Li, S. Jiang, W. Xiao, Y. Li, L. Tang, Y. Zhang, and D. Zhang, "Pressure-induced phase transformations in cubic Gd₂O₃," *J. Appl. Phys.* **106**, 073507 (2009).
- ³⁴P. Gribisch, J. Schmidt, H. J. Osten, and A. Fissel, "Influence of nanostructure formation on the crystal structure and morphology of epitaxially grown Gd₂O₃ on Si(001)," *Acta Cryst. B Struct. Sci. Cryst. Eng. Mater.* **75**, 59–70 (2019).
- ³⁵P. Zaumseil, "X-ray measurement of the tetragonal distortion of the oxide buffer layer in Ge/Pr₂O₃/Si(111) heteroepitaxial structures," *J. Phys. D: Appl. Phys.* **41**, 135308 (2008).
- ³⁶P. Zaumseil, "X-ray investigation of strained epitaxial layer systems by reflections in skew geometry," *J. Appl. Crystallogr.* **50**, 475–480 (2017).
- ³⁷D. Tetzlaff, T. F. Wietler, E. Bugiel, and H. J. Osten, "Carbon-mediated growth of thin, fully relaxed germanium films on silicon," *Appl. Phys. Lett.* **100**, 012108 (2012).
- ³⁸D. Tetzlaff, T. F. Wietler, E. Bugiel, and H. J. Osten, "Strain relaxation of thin Ge films on Si(001) grown by carbon-mediated epitaxy," *Semicond. Sci. Technol.* **378**, 254–258 (2013).
- ³⁹H. Genath, J. Schmidt, and H. J. Osten, "Analysis of thin germanium-rich SiGe layers on Si(111) substrates grown by carbon-mediated epitaxy," *J. Cryst. Growth* **535**, 125569 (2020).
- ⁴⁰H. Genath, J. Norberg, B. Wolpensinger, and H. J. Osten, "Investigation of the temperature stability of germanium-rich SiGe layers on Si(111) substrates," *Thin Solid Films* **763**, 139561 (2022).
- ⁴¹J. Wang, A. Laha, A. Fissel, D. Schwendt, R. Dargis, T. Watahiki, R. Shayduk, W. Braun, T. Liu, and H. J. Osten, "Structural and strain relaxation study of epitaxially grown nano-thick Nd₂O₃/Si(111) heterostructure," in *2009 4th IEEE International Conference on Nano/Micro Engineered and Molecular Systems (IEEE, 2009)*, pp. 436–440.
- ⁴²T. F. Wietler, A. Laha, E. Bugiel, M. Czernohorsky, R. Dargis, A. Fissel, and H. J. Osten, "Epitaxial growth of Gd₂O₃ on surfactant-mediated grown Ge films on Si(001) substrates," *Solid-State Electron.* **53**, 833–836 (2009).
- ⁴³K. R. Kiangte, J. S. Rathore, S. Das, R. S. Pokharia, J. Schmidt, H. J. Osten, A. Laha, and S. Mahapatra, "Molecular beam epitaxy and defect structure of Ge (111)/epi-Gd₂O₃ (111)/Si (111) heterostructures," *J. Appl. Phys.* **124**, 065704 (2018).
- ⁴⁴P. Shekhter, D. Schwendt, Y. Amouyal, T. F. Wietler, H. J. Osten, and M. Eizenberg, "Strain-induced phase variation and dielectric constant enhancement of epitaxial Gd₂O₃," *J. Appl. Phys.* **120**, 014101 (2016).
- ⁴⁵J. Wang, T. Liu, Z. Wang, E. Bugiel, A. Laha, T. Watahiki, R. Shayduk, W. Braun, A. Fissel, and H. J. Osten, "Epitaxial multi-component rare-earth oxide: A high-k material with ultralow mismatch to Si," *Mater. Lett.* **64**, 866–868 (2010).
- ⁴⁶N. Fairley, V. Fernandez, M. Richard-Plouet, C. Guillot-Deudon, J. Walton, E. Smith, D. Flahaut, M. Greiner, M. Biesinger, S. Tougaard, D. Morgan, and J. Baltrusaitis, "Systematic and collaborative approach to problem solving using X-ray photoelectron spectroscopy," *Appl. Surf. Sci. Adv.* **5**, 100112 (2021).
- ⁴⁷C. Powell, "X-ray Photoelectron Spectroscopy Database XPS, Version 4.1, NIST Standard Reference Database 20."
- ⁴⁸D. A. Shirley, "High-resolution X-ray photoemission spectrum of the valence bands of gold," *Phys. Rev. B* **5**, 4709–4714 (1972).
- ⁴⁹A. Proctor and P. M. A. Sherwood, "Data analysis techniques in X-ray photoelectron spectroscopy," *Anal. Chem.* **54**, 13–19 (1982).
- ⁵⁰D. Schmeisser, R. D. Schnell, A. Bogen, F. J. Himpsel, D. Rieger, G. Landgren, and J. F. Morar, "Surface oxidation states of germanium," *Surf. Sci.* **172**, 455–465 (1986).
- ⁵¹A. Fissel, Z. Elassar, O. Kirfel, E. Bugiel, M. Czernohorsky, and H. J. Osten, "Interface formation during molecular beam epitaxial growth of neodymium oxide on silicon," *J. Appl. Phys.* **99**, 074105 (2006).
- ⁵²X. Fan, H. Liu, and C. Fei, "Effect of post-deposition annealing on the interfacial chemical bonding states and band alignment of atomic layer deposited neodymium oxide on silicon," *Mater. Res. Express* **1**, 045005 (2014).
- ⁵³J. P. Baltrus and M. J. Keller, "Rare earth oxides Eu₂O₃ and Nd₂O₃ analyzed by XPS," *Surf. Sci. Spectra* **26**, 014001 (2019).
- ⁵⁴A. G. Shard, "Practical guides for x-ray photoelectron spectroscopy: Quantitative XPS," *J. Vac. Sci. Technol. A* **38**, 041201 (2020).
- ⁵⁵S. Tanuma, C. J. Powell, and D. R. Penn, "Calculations of electron inelastic mean free paths. II. Data for 27 elements over the 50–2000 eV range," *Surf. Interface Anal.* **17**, 911–926 (1991).
- ⁵⁶J. H. Scofield, "Hartree-slater subshell photoionization cross-sections at 1254 and 1487 eV," *J. Electron Spectros. Relat. Phenom.* **8**, 129–137 (1976).
- ⁵⁷D. J. Godbey and M. G. Ancona, "Ge profile from the growth of SiGe buried layers by molecular beam epitaxy," *Appl. Phys. Lett.* **61**, 2217–2219 (1992).
- ⁵⁸G. G. Jernigan, P. E. Thompson, and C. L. Silvestre, "Ge segregation during the initial stages of Si_{1-x}Ge_x alloy growth," *Appl. Phys. Lett.* **69**, 1894–1896 (1996).
- ⁵⁹G. G. Jernigan, P. E. Thompson, and C. L. Silvestre, "Quantitative measurements of Ge surface segregation during SiGe alloy growth," *Surf. Sci.* **380**, 417–426 (1997).
- ⁶⁰J. Felsche, *The Crystal Chemistry of the Rare-Earth Silicates* (Springer, 1973), Vol. 13, pp. 99–197.
- ⁶¹W.-H. Chang, S.-Y. Wu, C.-H. Lee, T.-Y. Lai, Y.-J. Lee, P. Chang, C.-H. Hsu, T.-S. Huang, J. R. Kwo, and M. Hong, "Phase transformation of molecular beam epitaxy-grown nanometer-thick Gd₂O₃ and Y₂O₃ on GaN," *ACS Appl. Mater. Interfaces* **5**, 1436–1441 (2013).
- ⁶²A. Fissel, M. Czernohorsky, and H. J. Osten, "Growth and characterization of crystalline gadolinium oxide on silicon carbide for high- application," *Superlattices Microstruct.* **40**, 551–556 (2006).
- ⁶³T.-H. Chiang, S.-Y. Wu, T.-S. Huang, C.-H. Hsu, J. Kwo, and M. Hong, "Single crystal Gd₂O₃ epitaxially on GaAs(111)A," *CrystEngComm* **16**, 8457 (2014).
- ⁶⁴A. Molle, C. Wiemer, M. D. N. K. Bhuiyan, G. Tallarida, and M. Fanciulli, "Epitaxial growth of cubic Gd₂O₃ thin films on Ge substrates," *J. Phys. Conf. Ser.* **100**, 042048 (2008).
- ⁶⁵Y.-L. Li, N.-F. Chen, J.-P. Zhou, S.-L. Song, L.-F. Liu, Z.-G. Yin, and C.-L. Cai, "Effect of the oxygen concentration on the properties of Gd₂O₃ thin films," *J. Cryst. Growth* **265**, 548–552 (2004).
- ⁶⁶W. F. Xiang, H. Ni, and H. B. Lu, "In situ RHEED analysis of epitaxial Gd₂O₃ thin films grown on Si (001)," *Appl. Phys. A* **110**, 423–426 (2013).
- ⁶⁷J. Coutures, A. Rouanet, R. Verges, and M. Foex, "Etude a Haute Température des Systèmes Formes par le Sesquioxyde de Lanthane et les Sesquioxydes de

Lanthanides. I. Diagrammes de Phases ($1400^{\circ}\text{C} < T < T_{\text{liquide}}$),” *J. Solid State Chem.* **17**, 171–182 (1976).

⁶⁸D. A. Hansen and J. B. Hudson, “The adsorption kinetics of molecular oxygen and the desorption kinetics of GeO on Ge(100),” *Surf. Sci.* **292**, 17–32 (1993).

⁶⁹A. Toriumi, S. Wang, C.-H. Lee, M. Yoshida, K. Kita, T. Nishimura, and K. Nagashio, “(Invited) Oxidation, diffusion and desorption in a Ge/GeO₂ system,” *ECS Trans.* **28**, 171–180 (2010).

⁷⁰S. K. Wang, K. Kita, C. H. Lee, T. Tabata, T. Nishimura, K. Nagashio, and A. Toriumi, “Desorption kinetics of GeO from GeO₂/Ge structure,” *J. Appl. Phys.* **108**, 054104 (2010).

⁷¹X. Li, Y. Noma, W. Song, T. Nishimura, and A. Toriumi, “Interface reaction kinetics in SiGe oxidation,” *Appl. Phys. Lett.* **115**, 232901 (2019).

⁷²I. Z. Mitrovic and S. Hall, “Rare earth silicate formation: A route towards high-k for the 22 nm node and beyond,” *J. Telecommun. Inf. Technol.* **4**, 51–60 (2009).

⁷³M. Copel, E. Cartier, and F. M. Ross, “Formation of a stratified lanthanum silicate dielectric by reaction with Si(001),” *Appl. Phys. Lett.* **78**, 1607–1609 (2001).

⁷⁴J. Chambers and G. N. Parsons, “Physical and electrical characterization of ultrathin yttrium silicate insulators on silicon,” *J. Appl. Phys.* **90**, 918–933 (2001).

⁷⁵H. Ono and T. Katsumata, “Interfacial reactions between thin rare-earth-metal oxide films and Si substrates,” *Appl. Phys. Lett.* **78**, 1832–1834 (2001).

⁷⁶X. Fan, H. Liu, C. Fei, B. Zhong, X. Wang, and Q. Wang, “Observation of optical properties of neodymium oxide with spectroscopic ellipsometry,” *J. Electron. Mater.* **44**, 2592–2597 (2015).

⁷⁷V. Narayanan, S. Guha, M. Copel, N. A. Bojarczuk, P. L. Flaitz, and M. Gribelyuk, “Interfacial oxide formation and oxygen diffusion in rare earth oxide–silicon epitaxial heterostructures,” *Appl. Phys. Lett.* **81**, 4183–4185 (2002).

⁷⁸S. van Elshocht, C. Adelman, T. Conard, A. Delabie, A. Franquet, L. Nyns, O. Richard, P. Lehnen, J. Swerts, and S. de Gendt, “Silicate formation and thermal stability of ternary rare earth oxides as high-k dielectrics,” *J. Vac. Sci. Technol. A* **26**, 724–730 (2008).

⁷⁹M. F. Bearad, C. D. Wirkus, and D. R. Wilder, “Diffusion of oxygen in selected monocrystalline rare earth oxides,” *J. Am. Ceram. Soc.* **51**, 643–647 (1968).

⁸⁰F. K. LeGoues, R. Rosenberg, T. Nguyen, F. Himpsel, and B. S. Meyerson, “Oxidation studies of SiGe,” *J. Appl. Phys.* **65**, 1724–1728 (1989).

⁸¹H. K. Liou, P. Mei, U. Gennser, and E. S. Yang, “Effects of Ge concentration on SiGe oxidation behavior,” *Appl. Phys. Lett.* **59**, 1200–1202 (1991).

⁸²M. K. Bera, S. Chakraborty, R. Das, G. K. Dalapati, S. Chattopadhyay, S. K. Samanta, W. J. Yoo, A. K. Chakraborty, Y. Butenko, L. Šiller,

M. R. C. Hunt, S. Saha, and C. K. Maiti, “Rapid thermal oxidation of Ge-rich Si_{1-x}Ge_x heterolayers,” *J. Vac. Sci. Technol. A* **24**, 84–90 (2006).

⁸³Z. Y. Xue, Z. F. Di, L. Ye, Z. Q. Mu, D. Chen, X. Wei, M. Zhang, and X. Wang, “Study of Ge loss during Ge condensation process,” *Thin Solid Films* **557**, 120–124 (2014).

⁸⁴F. Rozé, O. Gourhant, E. Blanquet, F. Bertin, M. Juhel, F. Abbate, C. Pribat, and R. Duru, “Oxidation kinetics of Si and SiGe by dry rapid thermal oxidation, in-situ steam generation oxidation and dry furnace oxidation,” *J. Appl. Phys.* **121**, 245308 (2017).

⁸⁵M. A. Rabie, Y. M. Haddara, and J. Carette, “A kinetic model for the oxidation of silicon germanium alloys,” *J. Appl. Phys.* **98**, 074904 (2005).

⁸⁶A. Terrasi, S. Scalese, R. Adorno, E. Ferlito, M. Spadafora, and E. Rimini, “Rapid thermal oxidation of epitaxial SiGe thin films,” *Mater. Sci. Eng. B* **89**, 269–273 (2002).

⁸⁷W. Song and A. Toriumi, “Study of SiGe oxidation kinetics for preferential SiO₂ formation under a low O₂ pressure condition,” *J. Appl. Phys.* **122**, 185301 (2017).

⁸⁸C.-T. Chang and A. Toriumi, “Preferential oxidation of Si in SiGe for shaping Ge-rich SiGe gate stacks,” in *2015 IEEE International Electron Devices Meeting (IEDM, Piscataway, NJ, 2015)*, pp. 21.5.1–21.5.4.

⁸⁹S. J. Kilpatrick, R. J. Jaccodine, and P. E. Thompson, “A diffusional model for the oxidation behavior of Si_{1-x}Ge_x alloys,” *J. Appl. Phys.* **81**, 8018–8028 (1997).

⁹⁰G. L. McVay and A. R. DuCharme, “Diffusion of Ge in SiGe alloys,” *Phys. Rev. B* **9**, 627–631 (1974).

⁹¹R. Kube, H. Bracht, J. L. Hansen, A. N. Larsen, E. E. Haller, S. Paul, and W. Lerch, “Composition dependence of Si and Ge diffusion in relaxed Si_{1-x}Ge_x alloys,” *J. Appl. Phys.* **107**, 073520 (2010).

⁹²P. Laitinen, A. Strohm, J. Huikari, A. Nieminen, T. Voss, C. Grodon, I. Riihimäki, M. Kummer, J. Aystö, P. Dendooven, J. Räisänen, and W. Frank, “Self-diffusion of ³¹Si and ⁷¹Ge in relaxed Si_{0.20}Ge_{0.80} layers,” *Phys. Rev. Lett.* **89**, 085902 (2002).

⁹³G. Lupina, T. Schroeder, J. Dabrowski, C. Wenger, A. U. Mane, H.-J. Müssig, P. Hoffmann, and D. Schmeisser, “Praseodymium silicate films on Si(100) for gate dielectric applications: Physical and electrical characterization,” *J. Appl. Phys.* **99**, 114109 (2006).

⁹⁴T. Hoai Le, K. Tang, S. Arnout, A. Malfliet, B. Blanpain, and M. Guo, “Thermodynamic assessment of the Nd₂O₃-CaO-SiO₂ ternary system,” *Calphad* **55**, 157–164 (2016).

⁹⁵R. Zhachuk, S. Teys, and J. Coutinho, “Strain-induced structure transformations on Si(111) and Ge(111) surfaces: A combined density-functional and scanning tunneling microscopy study,” *J. Chem. Phys.* **138**, 224702 (2013).

22 March 2024 06:55:37